Magnesium Dependence of the Amplified Conformational Switch in the Trans-Acting Hepatitis Delta Virus Ribozyme†

Rebecca A. Tinsley, Dinari A. Harris, and Nils G. Walter*

Department of Chemistry, The University of Michigan, 930 North University Avenue, Ann Arbor, Michigan 48109

Received March 16, 2004; Revised Manuscript Received May 14, 2004

ABSTRACT: The ability of divalent metal ions to participate in both structure formation and catalytic chemistry of RNA enzymes (ribozymes) has made it difficult to separate their cause and effect in ribozyme function. For example, the recently solved crystal structures of precursor and product forms of the cis-cleaving genomic hepatitis delta virus (HDV) ribozyme show a divalent metal ion bound in the active site that is released upon catalysis due to an RNA conformational change. This conformational switch is associated with a repositioning of the catalytically involved base C75 in the active-site cleft, thus controlling catalysis. These findings confirm previous data from fluorescence resonance energy transfer (FRET) on a trans-acting form of the HDV ribozyme that found a global conformational change to accompany catalysis. Here, we further test the conformational switch model by measuring the Mg^{2+} dependence of the global conformational change of the trans-acting HDV ribozyme, using circular dichroism and time-resolved FRET as complementary probes of secondary and tertiary structure formation, respectively. We observe significant differences in both structure and Mg^{2+} affinity of the precursor and product forms, in the presence and absence of 300 mM Na^+ background. The precursor shortens while the product extends with increasing Mg^{2+} concentration, essentially amplifying the structural differences observed in the crystal structures. In addition, the precursor has an ∼2-fold and ∼13-fold lower Mg^{2+} affinity than the product in secondary and tertiary structure formation, respectively. We also have compared the C75 wild-type with the catalytically inactive C75U mutant and find significant differences in global structure and Mg^{2+} affinity for both their precursor and product forms. Significantly, the Mg^{2+} affinity of the C75 wild-type is 1.7−2.1-fold lower than that of the C75U mutant, in accord with the notion that C75 is essential for a catalytic conformational change that leads to a decrease in the local divalent metal ion affinity and release of a catalytic metal. Thus, a consistent picture emerges in which divalent metal ions and RNA functional groups are intimately intertwined in affecting structural dynamics and catalysis in the HDV ribozyme.

Catalysis by RNA enzymes (ribozymes) is closely linked to their three-dimensional structure and conformational dynamics; both, in turn, are tied to the role of metal ions, particularly divalents, in neutralizing the negatively charged phosphoribose backbone. Therefore, studying the folding of ribozymes and the contributions of metal ions is key to our understanding of how RNA can become activated and poised for catalysis. It has been proposed that RNA folding is a two-step process, involving the formation of secondary structure, which then collapses into an ordered tertiary structure (*1*, *2*). Secondary structure formation in principle only requires a diffuse counterion atmosphere, consisting of monovalent or divalent metal ions, polyamines, and/or proteins, that screens the repulsion of the phosphates (*3*). In contrast, tertiary structure formation is characterized by a preference for divalent metal ions, which sometimes can, at least in part, be replaced by high concentrations of monovalents (*2*, *4*−*6*).

Divalent metal ions can contribute to ribozyme structure and function in more than one way. Aside from screening backbone charges and aiding tertiary structure formation, they also can be directly involved in a chemical reaction by acting as a cofactor to introduce functionalities that are scarce in RNA. For example, divalent metal ion hydroxo complexes may act as general base catalysts, activating a nucleophile via deprotonation, or their aqua complexes may serve as general acid catalysts to protonate the leaving group (*7*). Our perspective, particularly on the so-called "small" ribozymes, comprising the hammerhead, hairpin, *Neurospora* VS, and hepatitis delta virus (HDV)[1] ribozymes, has changed dramatically over the past few years from suspecting them as prime examples for metal ion catalysis to appreciating them

† This work was supported by NIH Grant GM62357 (N.G.W.), a University of Michigan Rackham Merit predoctoral fellowship (R.A.T. and D.A.H.), a predoctoral Merck/UNCF fellowship (D.A.H.), and an NIH supplement to Grant GM62357 (R.A.T.).

* To whom correspondence should be addressed. Phone: (734) 615-2060. Fax: (734) 647-4865. E-mail: nwalter@umich.edu.

[1] Abbreviations: CD, circular dichroism; DTT, dithiothreitol; EDTA, ethylenediaminetetraacetic acid; FRET, fluorescence resonance energy transfer; fwhm, full width at half-maximum; HDV, hepatitis delta virus; HPLC, high-performance liquid chromatography; SDS, sodium dodecyl sulfate; tr-FRET, time-resolved fluorescence resonance energy transfer.

10.1021/bi049471e CCC: $27.50
Published on Web 06/26/2004

as paradigms for RNA-mediated, metal-free catalysis (*2*, *4*, *7*).

HDV is a small pathogenic RNA satellite of the hepatitis B virus (HBV). Coinfection with HDV and HBV increases the severity of the disease symptoms associated with HBV, often leading to liver cirrhosis (*8*). Replication of the HDV RNA genome is proposed to occur through a double-rolling circle mechanism producing multimeric units of the complementary genomic and antigenomic RNA strands, both of which are able to self-cleave and religate into circular monomers (*8*). Cleavage activities in both the genome and antigenome depend on ~85-nucleotide RNA motifs, the two forms of the HDV ribozyme, which share an almost identical secondary structure that contains a double pseudoknot (*9*−*11*).

Self-cleavage activity of the HDV ribozyme has been proposed to occur via a general base/acid mechanism in which the 2′-hydroxyl group immediately 5′ to the cleavage site is deprotonated and attacks the scissile phosphate to form a 2′,3′-cyclic phosphate, leading to nucleophilic substitution of the 5′ oxyanion, which becomes protonated (*11*). Through a number of structural, biochemical, and mutagenesis studies it has been established that the base cytosine 75 (C75), or its antigenomic counterpart αC76 (α used to distinguish antigenomic numbering), plays an active role in this mechanism by serving as either the general base or the general acid (*11*). In particular, studies on the antigenomic HDV ribozyme suggest a role of αC76 as the general base catalyst that activates the 2′-OH for nucleophilic attack, based on the ribozyme's pH profile; the observed decrease in apparent reaction pK_a when a αC76A mutation is introduced; and the pH-dependent rescue of an αC76U mutation by high concentrations of imidazole (*12*−*14*). By contrast, the fact that the reaction pH profile of the genomic HDV ribozyme is inverted in the presence of 1 M NaCl and 1−100 mM EDTA has been interpreted as evidence for a kinetically indistinguishable model where the Mg^{2+} hydroxo complex acts as the general base whereas C75 acts as the general acid (*13*, *15*). Both models require the pK_a of C75 to be shifted from that of the free base (~4.2) to a value closer to neutrality in the context of the local structural environment in the transition state (*16*).

The crystal structure of the self-cleaved product form of the HDV ribozyme revealed that C75 is situated in the active-site cleft where it forms a hydrogen bond with the phosphate group of C22, providing a rationale for a shift in pK_a (*9*). Therefore, the assumption was made that the ribozyme precursor may structurally be almost identical to the product. However, the active-site cleft in the product crystal structure is tightly packed and does not provide an immediate trajectory for substrate exit. To probe for conformational rearrangements, we therefore used fluorescence resonance energy transfer (FRET) on a trans-acting form of the HDV ribozyme, which provided evidence for a significant conformational change upon catalysis. In particular, a sharp distance increase was observed between the termini of helices P2 and P4 after precursor cleavage and 5′ product dissociation (*17*). These global conformational changes were found to be dependent on the 5′ product sequence (*18*), consistent with the fact that there is a low sequence preference 5′ to the cleavage site (*19*, *20*). In addition, fluorescence spectroscopy of 2-aminopurine incorporated into C75's neighboring position, G76, showed a local conformational rearrangement to accompany the global structural change (*21*).

Recently, crystal structures of the precursor form of the self-cleaving HDV ribozyme have been solved (*22*), showing a global fold similar yet not identical to that of the product form. In addition, the precursor electron density provides evidence for a divalent metal ion in outer-sphere coordination to the −1 phosphate nonbridging oxygen and the 5′ oxygen of the leaving group, which places it in proximity to the ionizable C75, in accord with the observed linkage between Mg^{2+} concentration and pH dependence of activity (*5*, *15*). In agreement with our fluorescence data, upon catalysis and release of the 5′ product a significant local conformational change occurs in which the metal ion dissociates, thus controlling catalysis and making it essentially irreversible (*22*). Specifically, C75 shifts ~2 Å deeper into the active site, thus forming hydrogen bonds with the 5′-OH leaving group and a phosphate oxygen of C22, coupled with an inward movement of the P1 and P3 helices toward the center of the ribozyme. This led the authors to propose a refined catalytic mechanism where the hydrated metal ion acts as the general acid to protonate the 5′ oxyanion leaving group while C75 activates the 2′-OH, acting as the general base (*22*).

To further test the conformational switch model, we now have measured the Mg^{2+} dependence of the global conformational change of the trans-acting HDV ribozyme using circular dichroism and time-resolved FRET as complementary probes of secondary and tertiary structure formation, respectively. We observe significant differences in both structure and Mg^{2+} affinity of the precursor and product forms. The precursor shortens while the product extends with increasing Mg^{2+} concentration, in an amplification of the structural differences observed in the crystal structures of the cis-acting ribozyme. In addition, the precursor has an ~2-fold and ~13-fold lower Mg^{2+} affinity than the product in secondary and tertiary structure formation, respectively. Significantly, the Mg^{2+} affinity of the C75 wild-type is 1.7−2.1-fold lower than that of the C75U mutant, in accord with the notion that C75 is essential for the conformational switch that lowers the local divalent metal ion affinity and thus releases a catalytic metal. Our data therefore support a consistent picture in which Mg^{2+} ion(s) and C75 are intimately linked in affecting structural dynamics and catalysis in the HDV ribozyme.

MATERIALS AND METHODS

Preparation of RNA Oligonucleotides. RNA oligonucleotides (for sequences see Figure 1) were purchased from the Howard Hughes Medical Institute Biopolymer/Keck Foundation Biotechnology Resource RNA Laboratory at the Yale University School of Medicine (New Haven, CT). The RNA contained 2′-protection groups and was deprotected as suggested by the manufacturer (http://info.med.yale.edu/wmkeck/) (*23*, *24*). Deprotected RNA was purified by denaturing 20% polyacrylamide/8 M urea gel electrophoresis, diffusion elution into 0.5 M NH_4OAc, 0.1% SDS, and 0.1 mM EDTA overnight at 4 °C, chloroform extraction, ethanol precipitation, and C_8 reverse-phase HPLC with a linear acetonitrile gradient in triethylammonium acetate as described previously (*23*, *24*). To obtain the chemically

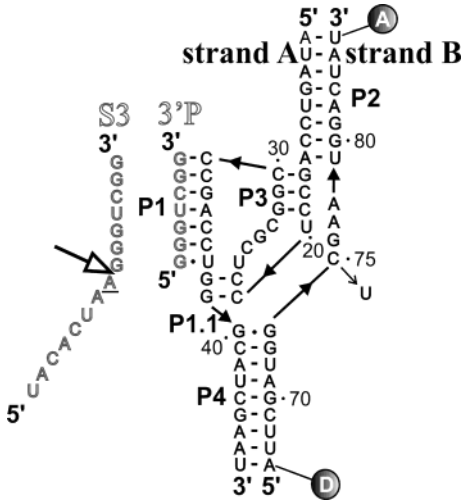

FIGURE 1: Synthetic three-strand trans-acting HDV ribozyme D1 employed as wild type in this study. Ribozyme strands A and B are shown in boldface type. Strand B contains the catalytically involved C75 that was mutated to U in some studies, as indicated. For FRET studies, a donor (D, fluorescein) and an acceptor (A, tetramethylrhodamine) fluorophore were attached to the 5′- and 3′ termini, respectively, of strand B, as indicated. The 3′ product strand (3′P) is shown in outline. Substrate S3 contains eight additional nucleotides 5′ to the cleavage site, which is indicated by an open arrow. To obtain a noncleavable substrate analogue (ncS3) for structural studies of the precursor form, the 2′-OH of the underlined −1 nucleotide was modified to a 2′-methoxy group.

blocked, noncleavable substrate analogue ncS3 for structural studies of the precursor form, the substrate was modified with a 2′-methoxy group at the cleavage site. The 3′ product (3′P) had the sequence 5′-GGGUCGG-3′. RNA concentrations were calculated from their absorption at 260 nm and corrected for the additional absorption of fluorescein and tetramethylrhodamine by using the relations $A_{260}/A_{492} = 0.3$ and $A_{260}/A_{554} = 0.49$, respectively.

Activity Assays. 5′-^{32}P-labeled substrates were prepared by phosphorylation with T4 polynucleotide kinase and [γ-^{32}P]-ATP. All activity assays were conducted under single-turnover (pre-steady-state) conditions. Standard buffer was 40 mM Tris-HCl, pH 7.5, either with or without 300 mM NaCl. The ribozyme was preannealed from strand A and twice the concentration of strand B in standard buffer supplemented with variable Mg^{2+} concentrations, by heating to 70 °C for 2 min and cooling to room temperature. After preincubation for at least 15 min at 25 °C, a trace (<4 nM) amount of 5′-^{32}P-labeled substrate (also in standard buffer supplemented with Mg^{2+}) was added to a saturating excess of 800 nM ribozyme (based on the strand A concentration), as previously described (*17*). Aliquots (5 μL) were taken at appropriate time intervals and the reaction was quenched with 10 μL of 80% formamide, 0.025% xylene cyanol, 0.025% bromophenol blue, and 50 mM EDTA. The 5′ cleavage product was separated from the uncleaved substrate by denaturing 20% polyacrylamide/8 M urea gel electrophoresis and was quantified and normalized to the sum of the substrate and product bands by use of a Storm 840 PhosphorImager with ImageQuant software (Molecular Dynamics). Time traces of product formation were fit to the single-exponential first-order rate equation $y = y_0 + A(1 - e^{-t/\tau})$, employing Marquardt−Levenberg nonlinear least-squares regression (Microcal Origin 7.0), where A is the amplitude and τ^{-1} is the pseudo-first-order rate constant k_{obs}. Mg^{2+} dependencies of this rate constant were fit to the binding equation:

$$k_{obs} = A_0 \pm k_{max}\frac{[Mg^{2+}]^n}{[Mg^{2+}]^n + Mg_{1/2}{}^n} \quad (1)$$

yielding the initial amplitude (or offset) A_0, the cleavage rate constant k_{max} under saturating Mg^{2+} concentrations, the apparent Mg^{2+} dissociation constant $Mg_{1/2}$, and the cooperativity constant n.

Time-Resolved FRET Measurements. The global structures of the wild-type and C75U mutant HDV ribozymes were studied under standard conditions as a function of Mg^{2+} concentration, by use of tr-FRET analysis of ribozyme complexes doubly labeled with fluorescein and tetramethylrhodamine (Figure 1), essentially as previously described (*17*). Specifically, the ribozyme−substrate (analogue) or −product complex (75 μL; 1 μM doubly labeled ribozyme strand B, 5 μM strand A, and either 10 μM substrate, noncleavable substrate analogue, or 3′ product), annealed by heating to 70 °C for 2 min and cooling to room temperature, was incubated at 25 °C for at least 15 min in standard buffer supplemented with 25 mM DTT and Mg^{2+}, as specified, in the presence or absence of 300 mM NaCl [in case of the cleavable substrate complex incubation in the presence of 11 mM Mg^{2+} is sufficient to bring cleavage to its final extent of typically ~77% (*17*)]. Time-resolved emission profiles of the donor fluorescein were then collected by previously described procedures based on time-correlated single-photon counting (*17*, *25*). Specifically, a frequency-doubled Nd:YVO4 laser (Spectra-Physics Millenia Xs-P, operated between 8 and 8.5 W) pumped a frequency-doubled, mode-locked Ti:sapphire laser (Spectra-Physics, operated at 1 W) that excited fluorescein at 492 nm with pulses 2 ps in width, picked down to 4 MHz. Detection of isotropic emission to >40 000 peak counts was performed under magic-angle polarizer conditions at 520 nm (10 nm band-pass interference filter). By use of a microchannel plate photomultiplier tube (Hamamatsu R3809U-50) feeding into an SPC-630 time-correlated single-photon counting card (Becker & Hickl), decays were collected into 4096 channels with a time increment of 12.20 ps/channel. An instrument response function was measured as the scattering signal from a dilute solution of nondairy coffee creamer to deconvolute the fluorescence decay data. To measure donor−acceptor distances, two time-resolved fluorescence decays were collected, with and without the acceptor in place. The fluorescein emission decay in the donor-only complex was used to extract the two or three intrinsic donor lifetimes τ_i with their fractional contributions α_i by a sum-of-exponentials fit. The data from the doubly labeled complex $I_{DA}(t)$ were then fit with a model for distance distributions:

$$I_{DA}(t) = \sum_k f_k \int P_k(R) \sum_i \alpha_i \exp\left\{-\frac{t}{\tau_i}\left[1 + \left(\frac{R_0}{R}\right)^6\right]\right\} dR$$

where the first sum refers to the number of distributions, either one or two, each with a fractional population f_k and a distance distribution $P_k(R)$. Distance distributions were modeled as weighted three-dimensional Gaussian functions:

$$P(R) = 4\pi R^2 c \exp[-a(R - b)^2]$$

where *a* and *b* are parameters that describe the shape of the distribution and *c* is a normalization constant. Fitting was performed by nonlinear least-squares regression, with *a*, *b*, and f_k for each distribution as adjustable parameters. An additional adjustable parameter was a small fraction of singly labeled complex (always <5%), accounting for photobleached acceptor fluorophore. The τ_i and α_i values from the donor-only decay were used under the assumption that each intrinsic donor lifetime is influenced independently by the presence of the acceptor at distance *R* and, by the distribution in *R*, is split into a lifetime distribution.

Mg^{2+} was titrated by incremental addition of 0.5 μL aliquots of appropriate $MgCl_2$ stock solutions in standard buffer supplemented with 25 mM DTT, taking into account the volume change; the volume at the end of any given titration increased by not more than 10%. In all cases, distance distribution fits were judged as good by their reduced χ^2 value (<1.2) and by evenly distributed residuals. To extract absolute distances, a value of 55 Å for the Förster distance R_0 of fluorescein and tetramethylrhodamine was used (*17*, *25*), assuming a value of $^2/_3$ for the orientation factor based on the high mobility of the fluorophores as evident from their low fluorescence anisotropies (*17*, *23*, *25*). The Mg^{2+} concentration dependence of the helix P2−P4 distance was fit to binding eq 1.

Circular Dichroism. Measurements were conducted on an Aviv 62DS spectrophotometer, equipped with a thermoprogrammable Peltier element, with a step size of 1 nm, a bandwidth of 1 nm, and a signal averaging time of 1.0 s. The preannealed ribozyme−noncleavable substrate analogue or ribozyme−product complex (1 mL; 2 μM stand A, 2 μM strand B, and 2 μM noncleavable substrate analogue or 3′-product) were incubated at 25 °C for at least 15 min in standard buffer. Mg^{2+} was titrated by incremental addition of 2 μL aliquots of appropriate $MgCl_2$ stock solutions in standard buffer, taking into account the volume change; the volume at the end of any given titration increased by not more than 5%. Scans were acquired over the spectral range of 215−300 nm and the CD data at 260 nm were normalized to the RNA length by use of the following equation to derive the molar circular dichroic absorption:

$$\Delta\epsilon_{260} = \frac{\theta}{32\,980 C l N} \qquad (2)$$

where θ is the measured CD signal in millidegrees, *C* is the sample concentration in moles per liter, *l* is the cell path length in centimeters, and *N* is the number of nucleotides of the RNA (*26*). $\Delta\epsilon_{260}$ was then plotted against the Mg^{2+} concentration and fit to binding eq 1.

RESULTS

Full Secondary Structure Assembly of the Three-Strand HDV Ribozyme Precursor Requires Sufficient Charge Screening. Figure 1 shows the three-strand, fully synthetic, trans-acting ribozyme construct D1 used in our present studies. It has the distinct advantage over a cis-acting, one-strand construct that a donor−acceptor fluorophore pair for FRET measurements can easily be introduced at the 5′ and 3′ termini, respectively, of strand B; and that either a noncleavable substrate analogue or the 3′ product can be annealed to the two ribozyme strands to represent the ribozyme precursor and product forms, respectively (Figure 1). Employing this construct, we have previously shown that the trans-acting HDV ribozyme undergoes a global conformational change upon catalysis (*17*) that coincides with local structural rearrangements in the catalytic core (*21*) and depends in magnitude on the sequence 5′ to the cleavage site (*18*). In addition, we found the conformational changes associated with substrate binding and dissociation by this ribozyme to be associated with significant solvent kinetic isotope effects (KSIEs), challenging the commonly held view that a KSIE necessarily provides evidence for reaction chemistry to be rate-limiting in an RNA enzyme (*27*).

Charge screening by solvent metal cations is known to be crucial for the secondary and tertiary structure folding and function of RNA as a polyanionic biopolymer (*2*). While our previous studies were performed at a fixed Mg^{2+} concentration of 11 mM, here we set out to better understand the impact of Mg^{2+} ions on the observed conformational changes by determining global structural parameters over a broad range of Mg^{2+} concentrations. To determine the relative impact of monovalent ions on structure and function of the HDV ribozyme, we decided to compare Mg^{2+} titrations in the absence and presence of a background of Na^+. Upon initial time-resolved FRET (tr-FRET) analysis of the wild-type ribozyme−noncleavable substrate complex (precursor, assembled from 1 μM doubly labeled strand B, 5 μM strand A, and 10 μM noncleavable substrate analogue ncS3) in standard buffer (40 mM Tris-HCl, pH 7.5) supplemented with 25 mM DTT at 25 °C, in the absence of added monovalents or divalents, we found the donor lifetime distribution to fit considerably better with a bimodal, rather than a unimodal, Gaussian distance distribution (Figure 2A). We found that 90% of the RNA population is centered around a mean helix P2−P4 end-to-end distance of 32 Å (fwhm = 17 Å), while 10% of the population exhibits a mean distance of 54 Å (fwhm = 25 Å). The shorter distance of 32 Å is identical to the mean distance of strand B alone (data not shown), indicating that, with limited countercharge present, the anticipated secondary structure is only partially formed and strand B largely resides in a random coil. To determine the minimum cation concentration needed to completely convert strand B into the precursor complex, we performed Na^+ and Mg^{2+} titrations under standard conditions and followed the relative abundances of the two strand B populations by tr-FRET (*25*) (data not shown). We found that a concentration of 300 mM Na^+ or higher was required to yield a single distance distribution with a mean of 53 Å (fwhm = 24 Å) that was no longer improved in fit quality (judged by the χ^2 value and residuals) by introducing a second distance distribution (Figure 2A, middle). Similarly, a concentration of 1 mM Mg^{2+} is needed in the absence of monovalents to convert all of strand B into a unimodal non-random-coil distance distribution (Figure 2A, lowest panel). These cation concentrations (300 mM Na^+ with 0 mM Mg^{2+} and 0 mM Na^+ with 1 mM Mg^{2+}) therefore define the lower boundary conditions for our Mg^{2+} titrations of the wild-type precursor complex. Interestingly, the wild-type and C75U mutant product complexes, as well as the C75U precursor complex, yield single distance distributions in the absence

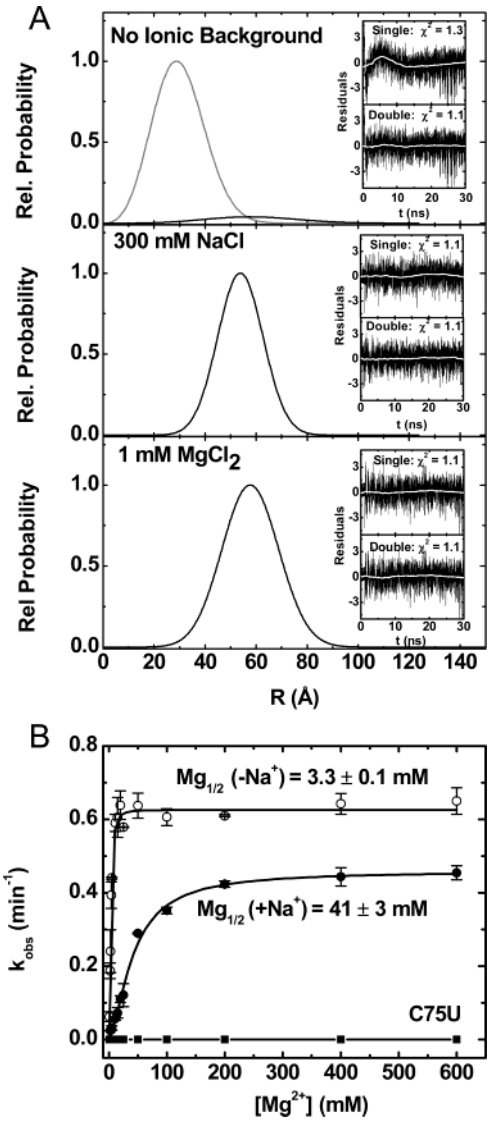

FIGURE 2: Folding and function of the trans-acting HDV ribozyme. (A) Fluorophore distance distributions of the ribozyme−noncleavable substrate (precursor) complex, as obtained by tr-FRET. Each panel shows the distance distribution of complex assembled from 1 μM strand B, 5 μM strand A, and 10 μM ncS3 in standard buffer (40 mM Tris-HCl, pH 7.5), supplemented with 25 mM DTT, in the absence of added salt (top panel) or in the presence of 300 mM NaCl (middle panel) or 1 mM $MgCl_2$ (bottom panel) at 25 °C. The following fit parameters were derived: (top) 90% of the population show $R_{obs}(1) = 32$ Å, fwhm(1) = 17 Å, while 10% of the population show $R_{obs}(2) = 54$ Å, fwhm(1) = 25 Å; (middle) $R_{obs} = 53$ Å and fwhm = 25 Å; (bottom) $R_{obs} = 52.5$ Å and fwhm = 24 Å. (Insets) Fit residuals (black lines) from unimodal (single) and bimodal (double) distributions, as indicated, and their running average over 100 data points (white lines) show that in the top panel, only a double distribution yields evenly distributed residuals and a low χ^2 value of 1.1, while in the middle and bottom panels, single distributions generate satisfactory fits. (B) Observed cleavage rate constants, k_{obs}, as a function of Mg^{2+} concentration under standard conditions (40 mM Tris-HCl, pH 7.5, at 25 °C) in the presence (●) or absence (○) of 300 mM NaCl. The experimental data were fit to binding eq 1 (see Materials and Methods) to yield the reported apparent Mg^{2+} dissociation constants $Mg_{1/2}$. (■) C75U mutant is inactive at all Mg^{2+} concentrations tested.

of added mono- and divalents (data not shown). This is consistent with the notion that these structures bind cations with higher affinities than the wild-type precursor form (see below) so that they fully assemble with relatively low charge screening.

Na^+ Inhibits Cleavage Activity of the Trans-Acting HDV Ribozyme. We compared the Mg^{2+} dependencies of the cleavage activity of our wild-type D1 HDV ribozyme under standard single-turnover conditions (800 nM ribozyme excess) in standard buffer (40 mM Tris-HCl, pH 7.5) at 25 °C, in the presence and absence of 300 mM NaCl (Figure 2B). In the absence of Na^+, the observed rate constants increase from 0.06 to 0.65 min^{-1} between 1 and 600 mM Mg^{2+}, yielding an apparent Mg^{2+} binding affinity of $Mg_{1/2} = 3.3 \pm 0.2$ mM (cooperativity constant $n = 1.79$) when fit to binding eq 1. Addition of 300 mM NaCl significantly decreases the observed rate constants throughout the entire Mg^{2+} range, with a maximum rate constant of only 0.45 min^{-1} and a $Mg_{1/2} = 41 \pm 3$ mM ($n = 2$) (Figure 2B). The apparent Mg^{2+} dissociation constants, $Mg_{1/2}$, show that Mg^{2+} binds with ~12-fold lower affinity in the presence of 300 mM Na^+ than in its absence, suggesting that Na^+ significantly inhibits cleavage activity of the trans-acting HDV ribozyme by competition with essential Mg^{2+} ions (*5*, *28*). As a specificity control we also tested the C75U mutant, in which the catalytically involved C75 is mutated to U, for cleavage activity under standard single-turnover conditions (800 nM ribozyme excess, 40 mM Tris-HCl, pH 7.5, at 25 °C). As expected, this variant does not exhibit any cleavage activity up to the highest Mg^{2+} concentration employed, 600 mM (Figure 2B).

Metal Ion Titrations Monitored by Time-Resolved FRET Show Substantial Differences in Mg^{2+}-Induced Conformational Changes between the Precursor and Product Forms. Fluorescence spectroscopy is a tool that is commonly used to probe folding, structure, and conformational dynamics of proteins and nucleic acids (*29*). Fluorescence resonance energy transfer (FRET), in particular, is a process in which excitation energy is transferred in a distance-dependent manner from a donor fluorophore to an acceptor fluorophore. It provides long-range distance information, typically in the 10−100 Å range, making it suitable for probing the global structure of nucleic acids by site-specifically attaching a suitable fluorophore pair (*23*, *24*, *30*, *31*). While steady-state FRET is a powerful tool for monitoring temporal changes in relative fluorophore distance, time-resolved FRET (tr-FRET) quantifies distances between donor and acceptor fluorophores to near-angstrom resolution and reports on global structure, intrinsic flexibility, and alternate conformations of an RNA (*32*).

Figure 3 shows in comparison Mg^{2+}-induced global conformational changes of C75 wild-type HDV ribozyme−noncleavable substrate analogue (ncS3, precursor) (panel A) and 3′ product (3′P) complexes (panel B). In particular, we monitored by tr-FRET the mean helix P2−P4 end-to-end distance in standard buffer at 25 °C as a function of Mg^{2+} concentration, in the presence or absence of 300 mM Na^+, as indicated (see Materials and Methods). In all cases we obtained unimodal distance distributions (data not shown), demonstrating that any alternate conformations constitute less than 5% of the RNA population. Upon raising the Mg^{2+} concentration, the ncS3 complex decreases in end-to-end distance from 52 to 50 Å (between 1 and 50 mM Mg^{2+}; $Mg_{1/2} = 1.5$ mM, $n = 1.14$) and from 53 to 50 Å (between 0 and 50 mM Mg^{2+}; $Mg_{1/2} = 3.6$ mM, $n = 1.18$), in the absence and presence of Na^+, respectively (Figure 3A). In contrast, the 3′P complex increases substantially in mean end-

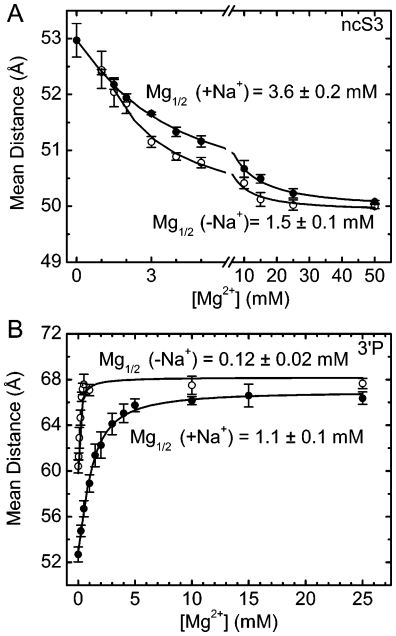

FIGURE 3: Mean helix P2−P4 end-to-end distance of the trans-acting HDV ribozyme in complex with (A) noncleavable substrate analogue ncS3 and (B) 3′ product (3′P), as a function of Mg^{2+} concentration in standard buffer (40 mM Tris-HCl, pH 7.5) supplemented with 25 mM DTT, in the presence (●) or absence (○) of 300 mM NaCl, at 25 °C. The experimental data were fit to binding eq 1 (Materials and Methods) to produce the reported apparent Mg^{2+} dissociation constants $Mg_{1/2}$.

to-end distance from 60 to 68 Å (between 0 and 25 mM Mg^{2+}; $Mg_{1/2} = 0.12$ mM, $n = 1.11$) and from 53 to 66 Å (between 0 and 25 mM Mg^{2+}; $Mg_{1/2} = 1.1$ mM, $n = 1.36$) in the absence and presence of Na^+, respectively (Figure 3B). Addition of 300 mM Na^+ thus has two main consequences: (i) The Mg^{2+} concentration necessary to induce global conformational changes in the precursor and 3′ product complexes is increased 2.4- and 9-fold, respectively. (ii) The Mg^{2+}-induced change in the helix P2−P4 distance is dampened for both the precursor and 3′ product complexes. These observations suggest that less folding-competent Na^+ ions compete with more folding-competent Mg^{2+} ions for binding sites that induce the observed RNA global conformational changes. In addition, comparing the Mg^{2+} dependencies of the precursor and 3′ product complexes shows that the 3′ product binds Mg^{2+} with a nearly 13-fold higher affinity than the precursor, whereas this distinction significantly decreases to only a 3.3-fold higher Mg^{2+} affinity in a background of 300 mM Na^+. The latter decrease is consistent with analysis of metal binding in the genomic cis-acting HDV ribozyme, which shows that Na^+ ions appear to bind more tightly to the product than the precursor form (*5*). It should also be noted that all cooperativity constants were close to unity during fitting with eq 1 (Figure 3), which is consistent with the notion that Mg^{2+} ions generally bind noncooperatively to the trans-acting HDV ribozyme.

Time-Resolved FRET Reveals Differences in Mg^{2+}-Induced Conformational Changes between the Wild-Type and C75U Mutant HDV Ribozymes. Mutagenesis studies show that changing the catalytically important C75 to a uracil (C75U mutation) completely ablates cleavage activity (*12*). A plausible reason is the absence of the exocyclic amino group that helps position C75 in the active-site cleft and, thus, in the proximity of the scissile phosphodiester by forming a hydrogen bond with the phosphate group of C22 (*9*). Consistent with this idea are recent crystallographic observations on the precursor form of the cis-acting HDV ribozyme by Doudna and co-workers (*22*), which suggest that the exocyclic amino group in fact is necessary for a conformational switch that ejects a catalytic Mg^{2+} ion and drives the cleavage reaction forward. To further test this model, we have used tr-FRET to address two specific questions about the wild-type and C75U mutant trans-acting HDV ribozymes: (i) Does the C75U mutant exhibit a different global structure than the C75 wild type in its precursor and/or 3′ product forms? (ii) Does the C75U mutant possess different metal-ion binding properties than the C75 wild type?

Table 1: Time-Resolved FRET Analysis of the C75 Wild-Type and C75U Mutant Ribozyme D1 in Its Complexes with Noncleavable Substrate Analogue NcS3, Cleavable Substrate S3, and 3′ Product 3′P[a]

parameter	ribozyme	D1	D1−ncS3	D1−S3	D1−3P
mean donor−acceptor distance (Å)	C75	54 ± 1	51 ± 1	63 ± 1	67 ± 1
	C75U	53 ± 1	55 ± 1	55 ± 1	70 ± 1
fwhm (Å)	C75	28 ± 1	20 ± 1	30 ± 1	33 ± 1
	C75U	26 ± 1	27 ± 1	26 ± 1	39 ± 1
χ^2	C75	1.1	1.1	1.1	1.1
	C75U	1.0	1.1	1.1	1.1

[a] Mean donor−acceptor distances and their full widths at half-maximum (fwhm) were measured in 40 mM Tris-HCl, pH 7.5, 11 mM $MgCl_2$, and 25 mM DTT at 25 °C. Errors were estimated from at least two independent measurements. χ^2 is the reduced chi-squared value as a measure of fit quality.

To this end, we have measured and compared the global conformations of our trans-acting C75 wild-type and C75U mutant HDV ribozymes in their precursor and 3′ product complexes (see Materials and Methods). First, tr-FRET was employed to measure the mean helix P2−P4 end-to-end distance of free ribozyme (D1), ribozyme−noncleavable substrate complex (precursor D1−ncS3), ribozyme−cleavable substrate complex (D1−S3), and ribozyme−3′ product complex (D1−3′P) under standard conditions (40 mM Tris-HCl, pH 7.5, 11 mM $MgCl_2$, and 25 mM DTT). The free C75 wild-type and C75U mutant ribozymes have similar mean distances of 54 Å (fwhm of 28 Å) and 53 Å (fwhm of 26 Å), respectively (Table 1). Upon formation of their (noncleavable) precursor complexes, however, the mean distance of the wild-type decreases to 51 Å (fwhm of 20 Å) while that of the mutant increases to 55 Å (fwhm of 27 Å) (Table 1). The 3′ product complexes also show a slight difference with mean distances of 67 Å (fwhm of 33 Å) and 70 Å (fwhm of 39 Å) for the C75 wild-type and C75U mutant, respectively (Table 1). Consistent with the fact that the wild type is catalytically active while the mutant is not, their ribozyme-cleavable substrate complexes significantly differ (their preincubation ensures that the final extent of cleavage is reached, see Materials and Methods); specifically, the wild type exhibits a mean distance of 63 Å (fwhm of 30 Å), similar to that of the 3′ product complex, while the C75U mutant has a mean distance of 55 Å (fwhm of 26 Å), identical to that of the uncleaved C75U precursor complex (Table 1).

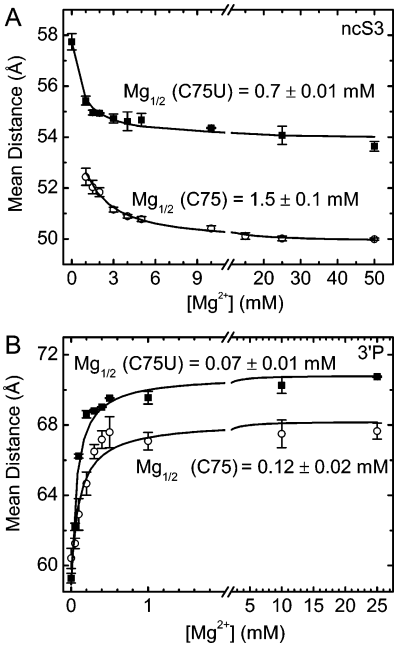

FIGURE 4: Mean helix P2−P4 end-to-end distance of C75 wild-type (○) and C75U mutant (■) ribozymes in complex with (A) noncleavable substrate analogue ncS3 and (B) 3′ product (3′P) as a function of Mg^{2+} concentration in standard buffer (40 mM Tris-HCl, pH 7.5) supplemented with 25 mM DTT, at 25 °C. The experimental data were fit to binding eq 1 (Materials and Methods) to produce the reported apparent Mg^{2+} dissociation constants $Mg_{1/2}$.

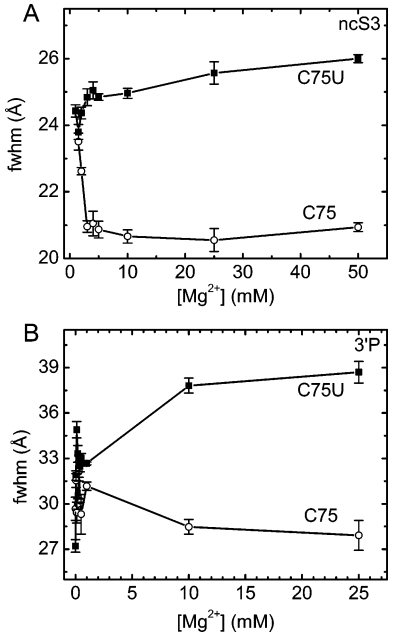

FIGURE 5: Mg^{2+} dependence of the full width at half-maximum (fwhm) of the measured distance distributions for the C75 wild-type (○) and C75U mutant (■) ribozymes in complex with (A) noncleavable substrate analogue ncS3 and (B) 3′ product (3′P) as a function of Mg^{2+} concentration in standard buffer (40 mM Tris-HCl, pH 7.5) supplemented with 25 mM DTT, at 25 °C.

Next, we compared tr-FRET-monitored Mg^{2+} titrations of the C75 wild-type and C75U mutant ribozymes in both their precursor and 3′ product forms. Figure 4A shows the mean helix P2−P4 end-to-end distance derived for the precursor forms under standard conditions (see Materials and Methods) as a function of Mg^{2+} concentration. With increasing [Mg^{2+}], the end-to-end distance of the C75 wild-type and C75U mutant ribozymes decreases slightly from 52 to 50 Å (between 1 and 50 mM Mg^{2+}; $Mg_{1/2} = 1.5$ mM, $n = 1.14$) and from 58 to 54 Å (between 0 and 50 mM Mg^{2+}; $Mg_{1/2} = 0.7$ mM, $n = 1.45$), respectively. Figure 4B shows the results of a similar titration of the 3′ product complexes. Here, the end-to-end distance of the C75 wild-type and C75U mutant ribozymes increases significantly from 60 to 68 Å (between 0 and 25 mM Mg^{2+}; $Mg_{1/2} = 0.12$ mM, $n = 1.11$) and from 59 to 70 Å (between 0 and 25 mM Mg^{2+}; $Mg_{1/2} = 0.07$ mM, $n = 1.22$), respectively. Taken together, these results show that the C75U mutant trans-acting HDV ribozyme generally has a larger helix P2−P4 distance combined with a higher Mg^{2+} binding affinity than the wild-type ribozyme, in both its precursor and 3′ product forms.

C75U Mutant Shows Increased Global Flexibility upon Mg^{2+} Binding. The full width at half-maximum (fwhm) of the helix P2−P4 end-to-end distance distribution, a measure of structural flexibility, is also derived through our tr-FRET analysis. It captures both the intrinsic global dynamics of the RNA between the fluorophore attachment sites and the local mobility of the fluorophores at the end of their attachment linkers (*32*). By directly comparing the C75 wild-type and C75U mutant ribozymes, which are identical except for the identity of the base in the 75 position, we can attribute differences in fwhm values primarily to the intrinsic global flexibility of the RNA. Figure 5 shows the fwhm values of the fluorophore distance distributions from our tr-FRET analysis as a function of Mg^{2+} concentration. Strikingly, both the precursor and 3′ product complexes of the C75 wild type significantly decrease in fwhm upon raising the Mg^{2+} concentration, while both the precursor and 3′ product complexes of the C75U mutant increase in fwhm. This suggests that the presence of C75 in the wild-type leads to a suppression of global structural flexibility upon Mg^{2+} binding, while lack of C75 in the mutant allows Mg^{2+} binding to induce higher intrinsic RNA flexibility.

Circular Dichroism Reveals Complementary Differences in Secondary Structure between the C75 Wild-Type and C75U Mutant Ribozymes. Circular dichroism (CD) spectroscopy is a common technique used to characterize changes in the amount of secondary and tertiary structure in RNA (*33*). Specifically, an increase in the CD signal at 260 nm is evidence for helix or secondary structure formation (*26*). To complement the global distance information derived from our tr-FRET analyses, we therefore examined CD spectra of the C75 wild-type precursor and 3′ product complexes before and after addition of 10 mM Mg^{2+} in standard buffer (40 mM Tris-HCl, pH 7.5; see Materials and Methods), in the presence or absence of 300 mM Na^+, as indicated in Figure 6. The CD spectra of the precursor and 3′ product complexes at 0 and 10 mM Mg^{2+} in a background of 300 mM Na^+ are virtually identical (Figure 6C,D), suggesting that, consistent with our tr-FRET data, 300 mM Na^+ is sufficient to fully form all secondary structure in the absence of Mg^{2+}. By contrast, and again consistent with our tr-FRET results, in the absence of Na^+ both the wild-type precursor and 3′ product complexes show significant changes in their CD spectra upon raising the Mg^{2+} concentration from 0 to 10 mM (Figure 6A,B), suggesting that the RNA secondary structure is not fully formed at low ionic strength.

To compare the Mg^{2+} dependence of secondary structure formation in the C75 wild-type and C75U mutant complexes,

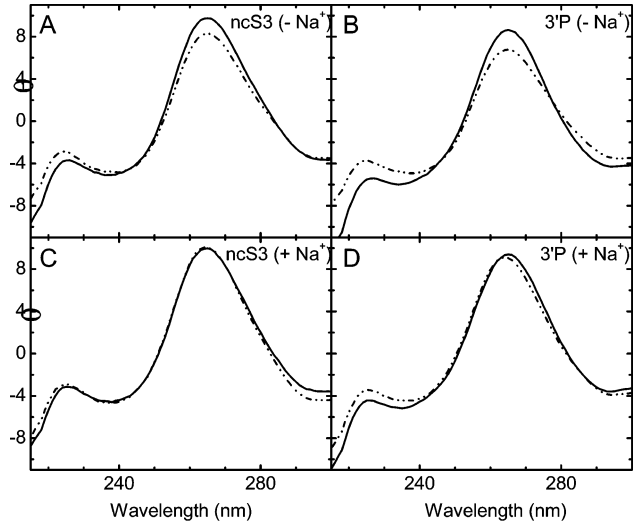

FIGURE 6: CD spectra from 215 to 300 nm for the wild-type trans-acting HDV ribozyme in complex with (A, C) noncleavable substrate analogue ncS3 and (B, D) 3′ product (3′P) at 0 mM (-••-) and 10 mM (—) Mg^{2+} in standard buffer (40 mM Tris-HCl, pH 7.5) in the absence (A, B) or presence (C, D) of 300 mM NaCl, as indicated, at 25 °C.

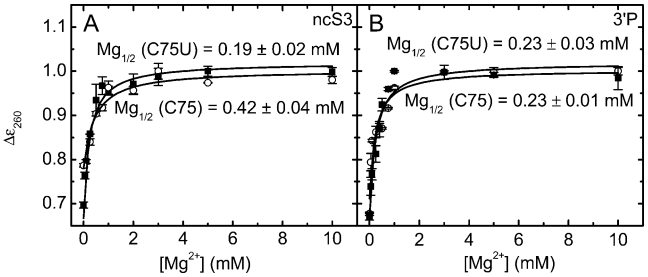

FIGURE 7: Mg^{2+} dependencies of the normalized CD signal at 260 nm for the C75 wild-type (○) and C75U mutant (■) ribozymes in complex with (A) noncleavable substrate analogue ncS3 and (B) 3′ product (3′P) in standard buffer (40 mM Tris-HCl and pH 7.5) at 25 °C. The experimental data were fit to binding eq 1 to produce the reported apparent Mg^{2+} dissociation constants $Mg_{1/2}$.

we performed CD-detected Mg^{2+} titrations in standard buffer (in the absence of Na^+; see Materials and Methods) on their precursor and product forms. Not surprisingly, the CD spectra of the C75U mutant complexes qualitatively resemble those of the wild type (data not shown). With increasing Mg^{2+} concentration, the normalized CD signal at 260 nm (see Materials and Methods) increases for both the C75 wild-type and C75U mutant precursor and product structures, indicative of additional secondary structure formation (Figure 7). The $Mg_{1/2}$ values, however, for the wild-type and mutant precursors differ by more than 2-fold at 0.42 mM ($n = 1.05$) and 0.19 mM ($n = 1.15$), respectively, while the $Mg_{1/2}$ values for their product forms are identical (0.23 mM, $n = 1.20$ and $n = 1.21$, respectively; Figure 7).

DISCUSSION

Most enzymes and their substrates undergo conformational changes that help position their functional groups for efficient catalysis (*34*). RNA enzymes are no exception, as many of them use this strategy to enhance their catalytic efficiency (*11*). Until recently it was assumed that the precursor, transition state, and product structures of the HDV ribozyme are largely identical (*9*, *35*). This assumption was based on the crystal structure of the self-cleaved 3′ product form, which lacks the 5′ product upstream of the cleavage site, a sequence that has been shown to have a significant impact on global conformation and catalytic activity of the HDV ribozyme (*18*−*20*). This impact may come as little surprise given that the catalytic core of the 3′ product is densely packed, providing limited exit trajectories for the 5′ sequence; thus the nature of the 5′ sequence may make it more or less conducive to structural rearrangements necessary for exit from the catalytic core. Consistent with this notion, we previously found the trans-acting HDV ribozyme to undergo a global conformational change upon catalysis (*17*) that coincides with local structural rearrangements in the catalytic core (*21*) and depends on the 5′ sequence (*18*). Recently solved precursor crystal structures of cis-acting HDV ribozymes complement this view as they show that conformational rearrangements occur upon catalysis, in which a possibly catalytically involved divalent metal ion is released as the critical C75 base repositions in the catalytic core (*22*). Thus, catalytic activity in the HDV ribozyme in fact appears to crucially depend on the conformational switch that accompanies catalysis (*22*).

To better understand how divalent metal ions and C75 contribute to conformational change and catalysis in the HDV ribozyme, we have used tr-FRET, in conjunction with cleavage assays and CD spectroscopy, to quantify the extent and functional relevance of Mg^{2+}-induced changes in the global structure and flexibility of C75 wild-type and C75U mutant precursor and product forms of a trans-acting HDV ribozyme (Figure 1). tr-FRET has previously been employed to accurately measure end-to-end distance distributions in other "small" ribozymes, such as the hairpin (*25*, *36*) and hammerhead ribozymes (*32*). Our results on the HDV ribozyme indicate that there are significant differences in global structure and metal ion affinity between the wild-type precursor and product forms, as well as between the wild-type and C75U mutant. The precursor shortens while the product extends with increasing Mg^{2+} concentration. In addition, the precursor has a 13- and 3.3-fold lower Mg^{2+} affinity than the product form in the absence and presence of 300 mM Na^+, respectively (Figure 3). Significantly, the Mg^{2+} affinity of the C75U mutant is 1.7−2.1-fold higher than that of the C75 wild type, and its structure is generally more extended than that of the wild type (Figure 4). This larger mean helix P2−P4 distance of the C75U mutant is accompanied by a more pronounced structural flexibility (Figure 5). Finally, CD spectroscopy shows that full secondary structure formation of the C75U mutant is associated with a 2.2-fold higher Mg^{2+} affinity, similar to the global structural changes monitored by tr-FRET (Figure 7). In the following we will interpret our results in light of recent crystallographic and biochemical evidence, yielding a consistent picture of the intimate relationship between divalent metal ions and RNA functional groups in structural dynamics and catalysis of the HDV ribozyme.

Trans-Acting HDV Ribozyme Amplifies Global Conformational Changes Observed in the Crystal Structures of the Cis-Acting Ribozyme. Comparison of the tr-FRET-derived helix P2−P4 end-to-end distances shows that the precursor is considerably shorter than the 3′ product complex, a difference that is significantly enhanced from ∼8 Å to as much as 18 Å upon increasing the Mg^{2+} concentration (in

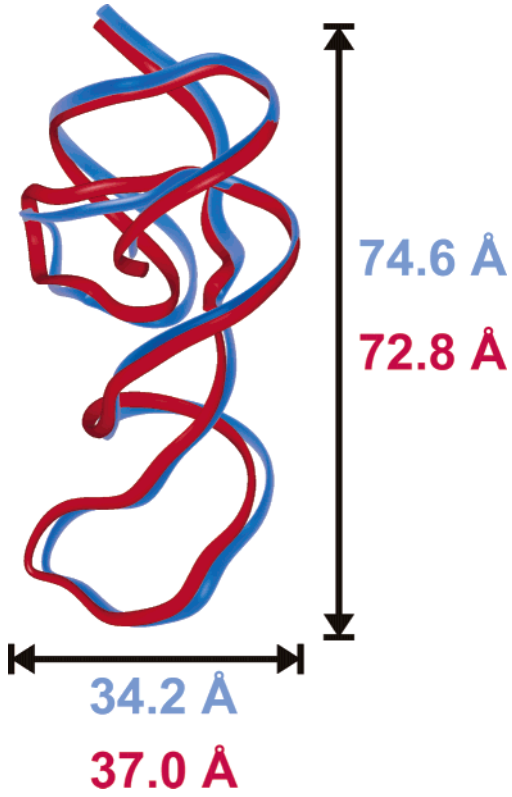

FIGURE 8: Backbone ribbon representation of the precursor (red, PDB ID 1SJ3) and 3′ product (blue, PDB ID 1CX0) forms of the genomic HDV ribozyme crystal structures. The distances between the phosphate of C26 in loop L3 and the phosphate of C36 in helix P1 (bottom) as well as those between the phosphate of U85 in helix P2 and the phosphate of C52 in helix P4 (right) were measured and are indicated.

the absence of Na^+; Figure 3). Strikingly, the same trend to global extension in the helical axis direction is observed upon self-cleavage of the cis-acting HDV ribozyme. Figure 8 illustrates this point on ribbon backbone representations of its precursor and product crystal structures. In the context of the crystal lattice, the cis-acting ribozyme exhibits only a muted end-to-end extension by ~2 Å upon conversion from precursor to 3′ product. However, the helix P2−P4 end-to-end distance in its 3′ product structure (74.6 Å) resembles that of the 3′ product complex of our trans-acting ribozyme at high Mg^{2+} concentration (68 Å), as observed previously (*17*) (please note that there are design differences in helices P2 and P4 between the two constructs, explaining some of the differences in absolute helix P2−P4 end-to-end distance).

This extension along the P2−P3 stack axis upon cleavage is accompanied by a constriction by ~3 Å along a perpendicular axis running through loop 3 and the catalytic core (Figures 1 and 8). The crystal structures give a strong indication for why these structural changes may occur; namely, that the 5′ sequence wedges with a sharp turn into the catalytic core between the two parallel helical stacks of the ribozyme, P2−P3 and P1−P1.1−P4, thus expanding the RNA in the perpendicular axis direction and shortening it in the direction of the helical stack. Upon cleavage and 5′ product dissociation, the 5′ sequence "wedge" is removed, the two helical stacks move in to close the catalytic core, and the 3′ product relaxes into its extended structure (Figures 1 and 8).

Why then is the cleavage-induced global extension along the helical stack axis amplified in the trans-acting ribozyme as compared to the crystal structures of the cis-acting ribozyme? One obvious difference between the crystallographic data and our solution-based tr-FRET assays is the absence of crystal lattice contacts in the latter. These contacts are necessary for crystallization and comprise U1A protein−protein interactions, engineered to anchor the bottom of P4; intermolecular stacking interactions between two G76s from neighboring RNA molecules, located in the joining sequence between P4 and P2; and intermolecular stacking interactions between the U1A binding loop of one RNA molecule and P2 of another, thus anchoring the top of P2 (Figure 1) (*35*). The strategic location of these intermolecular contacts may somewhat restrict the shortening in helix P2−P4 end-to-end distance in the precursor crystal structure. In addition, the trans-acting ribozyme lacks the short helical crossover that connects helices P1 and P2, thus tightly interlacing the P2−P3 and P1−P1.1−P4 helical stacks. In the absence of this crossover, which is severed in most trans-acting ribozymes, one may expect larger dynamics in the distance between, and relative orientation of, the P2−P3 and P1−P1.1−P4 helical stacks. Such larger dynamics and the resultant further expansion of the catalytic core between the two helical stacks would be expected to be particularly dramatic in the presence of the 5′ sequence of the precursor and is consistent with previous evidence from terbium(III)-mediated footprinting on the trans-acting ribozyme (*18*). It also may explain the ~10-fold slower cleavage rate generally observed for trans-acting ribozymes compared to cis-acting ones (*11*, *17*, *37*).

C75 Plays a Critical Role in the Catalytic Conformational Change. Figure 9 shows a schematic of the refined reaction mechanism of the HDV ribozyme as recently proposed by Doudna and co-workers (*22*) on the basis of the available crystallographic and biochemical evidence. The 2′-OH of the −1 nucleotide is deprotonated by the C75 base while a hydrated Mg^{2+} ion, coordinated to a phosphate oxygen of U23, acts as a general acid to protonate the 5′ oxyanion leaving group on G1. Upon catalysis, the 5′ product (including the scissile phosphate) and the divalent metal ion dissociate, while C75 moves deeper into the active site, essentially replacing the Mg^{2+} ion such that its exocyclic amino group and N3 now hydrogen-bond with the C22 phosphate oxygen and the 5′-OH of G1, respectively (Figure 9). The locations of the metal ion and C75 are directly resolved in the precursor and 3′ product crystal structures, and the proposed mechanism is further supported by mechanistic evidence that shows a strong inverse correlation between Mg^{2+} concentration and the apparent pK_a of C75, indicative of competition between Mg^{2+} binding and C75 protonation (*15*). According to this model of the reaction mechanism, the absence of C75's exocyclic amino group in the C75U mutant prohibits the conformational switch that repositions the base in the active site to drive the catalytic metal out and catalysis forward, causing the mutant to be catalytically inactive (Figure 9) (*22*).

Our comparative Mg^{2+} ion titrations of the C75 wild-type and C75U mutant trans-acting HDV ribozymes further support this model of the reaction mechanism. Specifically, the Mg^{2+} affinity of the wild type, as judged by following global folding as a function of Mg^{2+} concentration, is 1.7- and 2.1-fold lower than that of the C75U mutant in the

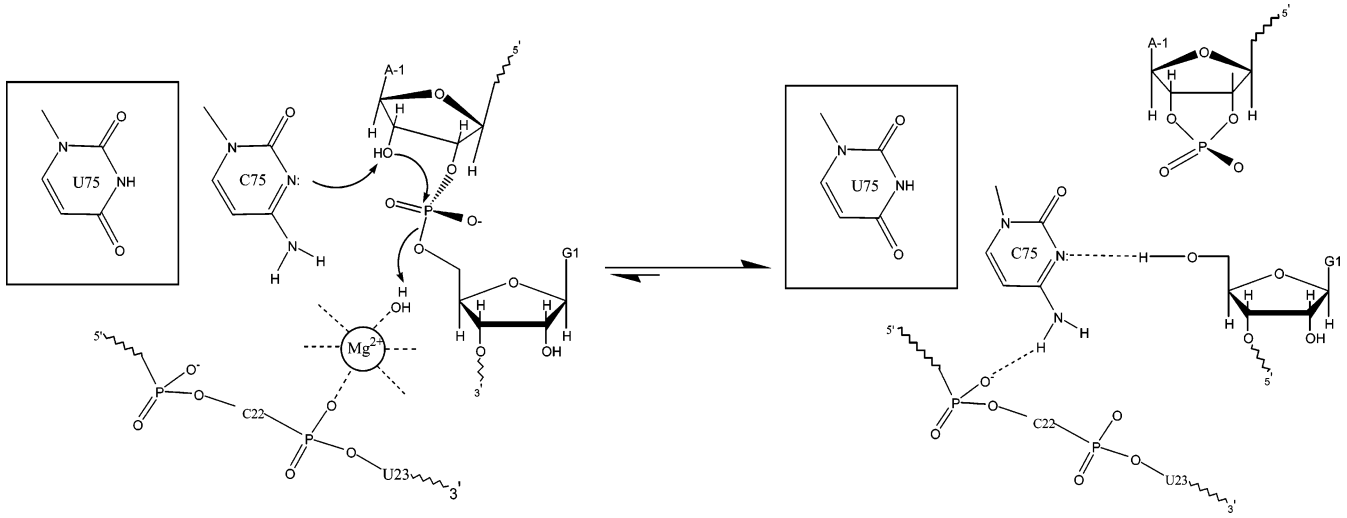

FIGURE 9: Reaction mechanism for general acid−base catalysis in the HDV ribozyme as recently proposed by Doudna and co-workers (*22*). Rotation about the 3′-O−P bond of the −1 nucleotide is proposed to bring its 2′-OH close to N3 of C75 for deprotonation and subsequent nucleophilic in-line attack on the scissile phosphate. Upon catalysis, a conformational change occurs in which C75 shifts downward to establish hydrogen bonds with the 5′-OH of G1 and a nonbridging phosphate oxygen of C22, thus replacing a hydrated Mg^{2+} ion that acts as general acid catalyst and then dissociates together with the 5′ product carrying the scissile phosphate. The base uracil, shown in the box, is unable to form this interaction due to the lack of an exocyclic amino group, rendering a C75U mutant inactive.

precursor and product complexes, respectively (Figure 4). This is consistent with the notion that C75 has a tendency, in both the precursor and product complexes, to lower the affinity for Mg^{2+}, presumably by local competition for a metal binding site(s). Furthermore, C75 compared to C75U leads to a structure with shorter helix P2−P4 end-to-end distance and lower global flexibility (Figures 4 and 5), providing evidence that C75 makes structural contacts inaccessible to a uracil that constrict the ribozyme rigidly along its helical stack axis. Taken together, our data implicate the exocyclic amino group of C75 in a significant tertiary structure interaction that is in competition with Mg^{2+} binding and is highly relevant to catalysis. A consistent picture thus emerges in which divalent metal ions and specific RNA functional groups are intimately linked in affecting structural dynamics and catalysis in the HDV ribozyme.

Differences in Mg^{2+} Affinities Monitored by CD, tr-FRET, and Functional Assays Suggest Multiple Roles for Divalents in Structure and Function of the HDV Ribozyme. Interestingly, the $Mg_{1/2}$ values obtained in our titrations monitored by CD spectroscopy (sensitive mainly to secondary structure formation), tr-FRET (sensitive mainly to global tertiary structure), and cleavage assays (sensitive to both structural and catalytic functionality) are quite distinct. This is best illustrated by comparing the $Mg_{1/2}$ values from CD, tr-FRET, and cleavage for the wild-type precursor complex, which are 0.42, 1.5, and 3.3 mM, respectively (compare Figures 2, 3, and 7). This suggests, first, that only relatively low charge screening by cations is needed to fully assemble the three strands of our trans-acting HDV ribozyme into a proper secondary structure. From the fact that 300 mM Na^+ have the same effect on the CD spectrum as millimolar Mg^{2+} concentrations (Figure 6) then derives the notion that the nature of the cationic countercharge (monovalent versus divalent) does not play a significant role in secondary structure formation. Second, the ∼3.6-fold higher $Mg_{1/2}$ observed by tr-FRET suggests that additional Mg^{2+} ions need to bind to organize the ribozyme's tertiary structure into a nativelike global fold. Third, the still 2.2-fold higher $Mg_{1/2}$ of cleavage provides evidence that at least one relatively low-affinity catalytic Mg^{2+} ion needs to bind to the ribozyme to activate it. Consistent with this notion, the cooperativity constant of the Mg^{2+} dependence of cleavage is close to 2 (Figure 2), in contrast to a cooperativity constant of tertiary structure formation close to 1, yielding a lower estimate of two Mg^{2+} ions involved in catalysis and suggesting that there are (at least) each one structural and one catalytic metal ion required for catalytic activity. Since the $Mg_{1/2}$ values derived from tr-FRET and cleavage assays are significantly increased in the presence of a background of 300 mM Na^+ (Figures 2 and 3), monovalent cations appear to act as competitive inhibitors of Mg^{2+} in tertiary structure folding and catalysis of the HDV ribozyme. These conclusions are very similar to those drawn by Bevilacqua and co-workers on the basis of catalytic activity and melting profiles of the cis-acting HDV ribozyme in the presence of mixtures of mono- and divalent metal ions (*5*, *28*). This complementarity of results validates both the trans- and cis-acting forms as important model systems to study catalysis by the genomic and antigenomic ribozymes derived from the hepatitis delta virus.

In summary, our results, in conjunction with previous biochemical and crystallographic data, demonstrate the close interrelation of the roles that metal ions and RNA functional groups play in structural dynamics and function by the HDV ribozyme. This is likely a general feature of RNA, as highlighted, for example, by recent advances in our understanding of catalysis by the hammerhead (*32*, *38*), hairpin (*39*), group I intron (*40*), and RNase P ribozymes (*41*, *42*), in addition to recent advances in our understanding of the nature of metal ion−RNA interactions (*7*, *43*, *44*). Future experiments are needed to provide further details on this interrelation, so that the full functional capability of RNA can be harnessed in biotechnological and medical applications.

ACKNOWLEDGMENT

We thank Jennifer Doudna and Ailong Ke for sharing crystal structure data and a manuscript prior to publication,

Jennifer Doudna for helpful suggestions on the C75U mutant, David Rueda for help with time-resolved FRET measurements and laser maintenance, Maria Rhodes and Jana Sefcikova for help with Figure 8, and all the members of the Walter laboratory for stimulating discussions and thoughtful suggestions.

REFERENCES

1. Brion, P., and Westhof, E. (1997) Hierarchy and dynamics of RNA folding, *Annu. Rev. Biophys. Biomol. Struct. 26*, 113−137.
2. Pyle, A. M. (2002) Metal ions in the structure and function of RNA, *J. Biol. Inorg. Chem. 7*, 679−690.
3. Misra, V. K., Shiman, R., and Draper, D. E. (2003) A thermodynamic framework for the magnesium-dependent folding of RNA, *Biopolymers 69*, 118−136.
4. Murray, J. B., Seyhan, A. A., Walter, N. G., Burke, J. M., and Scott, W. G. (1998) The hammerhead, hairpin and VS ribozymes are catalytically proficient in monovalent cations alone, *Chem. Biol. 5*, 587−595.
5. Nakano, S., Cerrone, A. L., and Bevilacqua, P. C. (2003) Mechanistic Characterization of the HDV Genomic Ribozyme: Classifying the Catalytic and Structural Metal Ion Sites within a Multichannel Reaction Mechanism, *Biochemistry 42*, 2982−2994.
6. Perez-Salas, U. A., Rangan, P., Krueger, S., Briber, R. M., Thirumalai, D., and Woodson, S. A. (2004) Compaction of a Bacterial Group I Ribozyme Coincides with the Assembly of Core Helices, *Biochemistry 43*, 1746−1753.
7. DeRose, V. J. (2003) Metal ion binding to catalytic RNA molecules, *Curr. Opin. Struct. Biol. 13*, 317−324.
8. Lai, M. M. (1995) The molecular biology of hepatitis delta virus, *Annu. Rev. Biochem. 64*, 259−286.
9. Ferre-D'Amare, A. R., Zhou, K., and Doudna, J. A. (1998) Crystal structure of a hepatitis delta virus ribozyme, *Nature 395*, 567−574.
10. Wadkins, T. S., Perrotta, A. T., Ferre-D'Amare, A. R., Doudna, J. A., and Been, M. D. (1999) A nested double pseudoknot is required for self-cleavage activity of both the genomic and antigenomic hepatitis delta virus ribozymes, *RNA 5*, 720−727.
11. Shih, I. H., and Been, M. D. (2002) Catalytic strategies of the hepatitis delta virus ribozymes, *Annu. Rev. Biochem. 71*, 887−917.
12. Perrotta, A. T., Shih, I., and Been, M. D. (1999) Imidazole rescue of a cytosine mutation in a self-cleaving ribozyme, *Science 286*, 123−126.
13. Wadkins, T. S., Shih, I., Perrotta, A. T., and Been, M. D. (2001) A pH-sensitive RNA tertiary interaction affects self-cleavage activity of the HDV ribozymes in the absence of added divalent metal ion, *J. Mol. Biol. 305*, 1045−1055.
14. Shih, I. H., and Been, M. D. (2001) Involvement of a cytosine side chain in proton transfer in the rate-determining step of ribozyme self-cleavage, *Proc. Natl. Acad. Sci. U.S.A. 98*, 1489−1494.
15. Nakano, S., Chadalavada, D. M., and Bevilacqua, P. C. (2000) General acid−base catalysis in the mechanism of a hepatitis delta virus ribozyme, *Science 287*, 1493−1497.
16. Bevilacqua, P. C., Brown, T. S., Nakano, S., and Yajima, R. (2004) Catalytic roles for proton transfer and protonation in ribozymes, *Biopolymers 73*, 90−109.
17. Pereira, M. J., Harris, D. A., Rueda, D., and Walter, N. G. (2002) Reaction pathway of the trans-acting hepatitis delta virus ribozyme: a conformational change accompanies catalysis, *Biochemistry 41*, 730−740.
18. Jeong, S., Sefcikova, J., Tinsley, R. A., Rueda, D., and Walter, N. G. (2003) Trans-acting hepatitis delta virus ribozyme: catalytic core and global structure are dependent on the 5′ substrate sequence, *Biochemistry 42*, 7727−7740.
19. Deschenes, P., Lafontaine, D. A., Charland, S., and Perreault, J. P. (2000) Nucleotides −1 to −4 of hepatitis delta ribozyme substrate increase the specificity of ribozyme cleavage, *Antisense Nucleic Acid Drug. Dev. 10*, 53−61.
20. Shih, I., and Been, M. D. (2001) Energetic contribution of nonessential 5′ sequence to catalysis in a hepatitis delta virus ribozyme, *EMBO J. 20*, 4884−4891.
21. Harris, D. A., Rueda, D., and Walter, N. G. (2002) Local conformational changes in the catalytic core of the trans-acting hepatitis delta virus ribozyme accompany catalysis, *Biochemistry 41*, 12051−12061.
22. Ke, A., Zhou, K., Ding, F., Cate, J. H. D., and Doudna, J. A. (2004) A conformational switch controls hepatitis delta virus ribozyme catalysis, *Nature 429*, 201−205.
23. Walter, N. G. (2001) Structural dynamics of catalytic RNA highlighted by fluorescence resonance energy transfer, *Methods 25*, 19−30.
24. Walter, N. G. (2002) Probing RNA structural dynamics and function by fluorescence resonance energy transfer (FRET), *Curr. Protocols Nucleic Acid Chem. Chapter 11.10*, 11.10.1−11.10.23.
25. Walter, N. G., Burke, J. M., and Millar, D. P. (1999) Stability of hairpin ribozyme tertiary structure is governed by the interdomain junction, *Nat. Struct. Biol. 6*, 544−549.
26. Sosnick, T. R., Fang, X., and Shelton, V. M. (2000) Application of circular dichroism to study RNA folding transitions, *Methods Enzymol. 317*, 393−409.
27. Tinsley, R. A., Harris, D. A., and Walter, N. G. (2003) Significant kinetic solvent isotope effects in folding of the catalytic RNA from the hepatitis delta virus, *J. Am. Chem. Soc. 125*, 13972−13973.
28. Nakano, S., Proctor, D. J., and Bevilacqua, P. C. (2001) Mechanistic characterization of the HDV genomic ribozyme: assessing the catalytic and structural contributions of divalent metal ions within a multichannel reaction mechanism, *Biochemistry 40*, 12022−12038.
29. Walter, N. G., and Burke, J. M. (2000) Fluorescence assays to study structure, dynamics, and function of RNA and RNA−ligand complexes, *Methods Enzymol. 317*, 409−440.
30. Walter, N. G., Harris, D. A., Pereira, M. J., and Rueda, D. (2002) In the fluorescent spotlight: Global and local conformational changes of small catalytic RNAs, *Biopolymers 61*, 224−242.
31. Klostermeier, D., and Millar, D. P. (2002) Time-resolved fluorescence resonance energy transfer: a versatile tool for the analysis of nucleic acids, *Biopolymers 61*, 159−179.
32. Rueda, D., Wick, K., McDowell, S. E., and Walter, N. G. (2003) Diffusely bound Mg^{2+} ions slightly reorient stems I and II of the hammerhead ribozyme to increase the probability of formation of the catalytic core, *Biochemistry 42*, 9924−9936.
33. Shelton, V. M., Sosnick, T. R., and Pan, T. (1999) Applicability of urea in the thermodynamic analysis of secondary and tertiary RNA folding, *Biochemistry 38*, 16831−16839.
34. Fersht, A. (1999) *Structure and Mechanism in Protein Science*, Freeman, New York.
35. Ferre-D'Amare, A. R., and Doudna, J. A. (2000) Crystallization and structure determination of a hepatitis delta virus ribozyme: use of the RNA-binding protein U1A as a crystallization module, *J. Mol. Biol. 295*, 541−556.
36. Klostermeier, D., and Millar, D. P. (2001) Tertiary structure stability of the hairpin ribozyme in its natural and minimal forms: different energetic contributions from a ribose zipper motif, *Biochemistry 40*, 11211−11218.
37. Shih, I., and Been, M. D. (2000) Kinetic scheme for intermolecular RNA cleavage by a ribozyme derived from hepatitis delta virus RNA, *Biochemistry 39*, 9055−9066.
38. Dunham, C. M., Murray, J. B., and Scott, W. G. (2003) A helical twist-induced conformational switch activates cleavage in the hammerhead ribozyme, *J. Mol. Biol. 332*, 327−336.
39. Bokinsky, G., Rueda, D., Misra, V. K., Rhodes, M. M., Gordus, A., Babcock, H. P., Walter, N. G., and Zhuang, X. (2003) Single-molecule transition-state analysis of RNA folding, *Proc. Natl. Acad. Sci. U.S.A. 100*, 9302−9307.
40. Rangan, P., and Woodson, S. A. (2003) Structural requirement for Mg^{2+} binding in the group I intron core, *J. Mol. Biol. 329*, 229−238.
41. Kurz, J. C., and Fierke, C. A. (2002) The affinity of magnesium binding sites in the *Bacillus subtilis* RNase P x pre-tRNA complex is enhanced by the protein subunit, *Biochemistry 41*, 9545−9558.
42. Brannvall, M., Pettersson, B. M., and Kirsebom, L. A. (2003) Importance of the +73/294 interaction in *Escherichia coli* RNase P RNA substrate complexes for cleavage and metal ion coordination, *J. Mol. Biol. 325*, 697−709.
43. Lilley, D. M. (2003) The origins of RNA catalysis in ribozymes, *Trends Biochem. Sci. 28*, 495−501.
44. Draper, D. E. (2004) A guide to ions and RNA structure, *RNA 10*, 335−343.

BI049471E